Catal Lett (2015) 145:596–605
DOI 10.1007/s10562-014-1454-7

NaCl-Promoted CuO–RuO_2/SiO_2 Catalysts for Propylene Epoxidation with O_2 at Atmospheric Pressures: A Combinatorial Micro-reactor Study

Şule Kalyoncu · Derya Düzenli · Isik Onal · Anusorn Seubsai · Daniel Noon · Selim Senkan · Zafer Say · Evgeny I. Vovk · Emrah Ozensoy

Received: 16 September 2014 / Accepted: 24 November 2014 / Published online: 9 December 2014

Abstract A combinatorial approach is used to investigate several alkali metals promoted Cu–Ru binary oxide catalysts with improved catalytic performance in the propylene partial oxidation. 2 %Cu/5 %Ru/c–SiO_2 catalyst had the best yield with high propylene conversion and propylene oxide (PO) selectivity. Among the promoters screening in the study, NaCl promotion significantly increased the PO selectivity accompanied by some attenuation in the total propylene conversion. It was proposed that binary oxide catalysts revealed a greater number of exposed catalytically active adsorption sites as compared to monometallic oxide counterparts according to XPS and FTIR results. Besides NaCl addition alters the structure, yielding a significantly improved PO selectivity without any change in the particle size of Cu and Ru oxide according to XRD analysis.

Keywords Propylene · Epoxidation · Ru · Cu · SiO_2

Ş. Kalyoncu · D. Düzenli · I. Onal (✉)
Department of Chemical Engineering, Middle East Technical University, Ankara 06800, Turkey
e-mail: ional@metu.edu.tr

A. Seubsai
Department of Chemical Engineering, Kasetsart University, Bangkok 10900, Thailand

D. Noon · S. Senkan
Department of Chemical and Biomolecular Engineering, UCLA, Los Angeles, CA 90095-1592, USA

Z. Say · E. I. Vovk · E. Ozensoy
Department of Chemistry, Bilkent University, Ankara 06800, Turkey

E. I. Vovk
Boreskov Institute of Catalysis, Novosibirsk 630090, Russian Federation

1 Introduction

Propylene oxide (PO) is a very important chemical feedstock for the production of a wide variety of commodity chemicals, such as polyether polyols and propylene glycol [1]. Currently, chlorohydrin and organic hydroperoxide processes are two of the commonly used industrial processes for PO synthesis in the chemical industry. These processes lead to the generation of a large amount of waste water and organic byproducts. Thus, they are not preferable due to their environmental and economical drawbacks [2]. Because of the deficiencies of the aforementioned PO production processes, novel methods of producing PO have been explored which included direct oxidation of propylene using various catalytic systems and proper oxidants, such as H_2O_2 [3–5] O_2–H_2 gas mixture [6–9] and N_2O [10, 11]. However, high costs of these oxidants restrict the commercialization of these processes. Therefore, the direct gas-phase epoxidation of propylene to PO by molecular oxygen has been a focus of interest as an attractive alternative from both economical and environmental standpoints.

The recent discovery of the highly active Au/TiO_2 catalysts in various catalytic reactions led to the use of Au in conjunction with other reducible metal oxide support materials [7–9, 12–15]. However, since highly selective Au catalysts typically exhibit low propylene conversion and require hydrogen co-feeding, such catalysts are industrially less promising for PO production [8]. Successful results obtained from modified Ag catalysts in the gas phase epoxidation of ethylene by molecular oxygen led to many studies on propylene epoxidation over different support materials and modifiers [16–28]. However the conversion and the selectivity of Ag-based catalysts in PO production were lower than those for ethylene oxide production as a

result of the existence of allylic hydrogen in propylene. The allylic C–H bonds in propylene were reported to be much more active towards oxidation than vinyl C–H bonds in ethylene which is in line with the lower selectivity values observed in propylene epoxidation catalysis [29]. Furthermore, surface chemistry studies on Ag and Cu single crystal surfaces suggested that Cu is more selective than Ag for the epoxidation of alkenes having allylic C–H bonds [30].

The reason behind the higher epoxidation activity of Cu with respect to that of Ag was explained by the lower basicity of oxygen adsorbed over Cu metal [31]. As a supporting study, the effect of the oxygen basicity on PO selectivity was investigated by Kızılkaya et al. [32]. In this DFT study over Cu and Cu–Ru catalytic systems, Kızılkaya et al. proposed that because of the higher basicity of atomic oxygen adsorbed over Cu–Ru, the scission of allylic hydrogen of propylene occurs with high probability (much lower activation barrier) as compared to the formation of the PO intermediate. Several studies in the literature focused on the active oxidation state of Cu in epoxidation reactions. Vaughan et al. proposed that Cu^0 species in highly dispersed atomic-like form are the active sites in epoxidation [33]. On the other hand, Zhu et al. claimed that Cu^+ is the active form [34]. Onal et al. suggested that isolated ionic Cu^{2+} species were responsible for propylene epoxidation by O_2 [35].

The studies reported in the literature showed that bimetallic or multimetallic catalytic systems for the propylene epoxidation reaction often show superior catalytic properties in comparison to monometallic systems [35–37]. Onal et al. reported that PO yield is increased by several folds for Ag–Cu bimetallic catalysts because of a synergistic effect [35].In addition, Kahn et al. reported that the PO formation rates of Cu–Mn bimetallic catalysts were about five times higher than the corresponding monometallic catalysts [36]. Although bimetallic catalysts have been commonly employed in propylene epoxidation, most of these catalytic systems suffered from low propylene conversion. Seubsai and co-workers have reported a new SiO_2-supported trimetallic RuO_2–CuO_x–NaCl catalyst with the highest PO yield (40–50 % PO selectivity at 10–20 % conversion for the direct epoxidation of propylene by molecular oxygen under atmospheric pressures [37]. Furthermore, He et al. reported that Cs^+ modified CuO_x/SiO_2 catalyst under O_2-rich atmosphere gave 2.6 % PO yield (34 % selectivity @ 7.5 % conversion) which is close to the performance of the aforementioned trimetallic catalyst performance mentioned above [38].

In this study, using a combinatorial approach, RuO_2 and CuO based monometallic and binary oxide catalytic systems were prepared on various SiO_2 support materials in the presence of alkali promoters such as Na, K and Li for the direct epoxidation of propylene to PO via molecular oxygen at atmospheric pressures. In order to find a highly active and a selective catalyst, a sequential combinatorial optimization approach was followed starting with the exploration of the optimum Ru and Cu relative loadings, followed by the selection of the optimum silica support material and finally the selection of the most effective promoter.

2 Experimental

2.1 Catalyst Preparation

SiO_2-supported mono and bimetallic heterogeneous catalysts were prepared using different synthesis methods. Silica support materials were either synthesized by using a template (t-SiO_2) or a sol–gel method (s-SiO_2) or they were directly acquired commercially (c-SiO_2, Alfa Aesar, surface area 97 $m^2\ g^{-1}$). The metal salts were also loaded on SiO_2 either by adding the metal salts to the synthesis mixture during the support material preparation step or by the incipient wetness impregnation of these salts onto the silica support material.

Catalysts containing s-SiO_2 were prepared using the following precursors: tetraethyl orthosilicate (TEOS, 99 % purity, Fluka), ethanol (EtOH), deionized water, 1 M HNO_3, 0.5 M NH_4OH, copper nitrate ($Cu(NO_3)_2$, 99.99 % purity, Aldrich) and ruthenium (III) chloride hydrate ($RuCl_3{\cdot}xH_2O$, 99.98 % purity, Aldrich). The corresponding molar ratios of the chemicals used in the s-SiO_2 synthesis was TEOS:EtOH:HNO_3:H_2O:NH_4OH = 1:20:1:13:0.5. Cu and Ru metal loadings were also varied between 0 and 2 wt% and 0 and 5 wt%, respectively. In the s-SiO_2 synthesis, TEOS, HNO_3, ethanol and water were mixed together at room temperature and then heated at 80–85 °C for 2 h. During heating, the solution was constantly stirred by a magnetic stirrer and refluxed. Then, metal precursors were added into the mixture and the mixture was stirred for 1 h under these conditions. In order to obtain the gel, NH_4OH was added to the synthesis mixture. After aging the gel for 24 h under ambient conditions, catalysts were dried at 120 °C and further calcined at 550 °C for 5 h. Pure s-SiO_2 material was prepared by skipping metal addition steps for wet impregnation method.

Catalysts containing t-SiO_2 were synthesized according to the method given in the literature [39].The chemicals used in synthesis of t-SiO_2 were: TEOS, 15.8 M HNO_3, dodecylamine (DDA, 98 % purity, Fluka), EtOH and water. The corresponding molar ratios of EtOH:HNO_3:H_2O:DDA used in the synthesis were 6.54:0.02:36.3:0.27. During the synthesis of the t-SiO_2, DDA, HNO_3 and deionized water were mixed and stirred for 1 h. Then TEOS and EtOH were added to the above mixture. The mixture was further stirred for 4 h at room temperature. Resulting mixture was aged under ambient conditions for

18 h. Next, the product was filtered, dried at 70 °C for 24 h and further calcined at 650 °C for 3 h. The synthesized t-SiO_2 material was used to prepare Ru–Cu bimetallic oxides system by wet impregnation method.

Wet impregnation method was also employed in order to synthesize Ru–Cu catalysts using s-SiO_2, t-SiO_2 and c-SiO_2 support materials. The prepared sample was dried at 120 °C for 12 h and further calcined. s-SiO_2 and c-SiO_2 supported catalysts were calcined at 550 °C for 5 h while t-SiO_2 sample was calcined at 650 °C for 3 h. In the synthesis of alkali-promoted catalysts, sodium nitrate ($NaNO_3$), lithium chloride (LiCl), potassium nitrate (KNO_3), sodium chloride (NaCl), and potassium acetate (KAc) salts were used as promoters. The desired amount of alkali salts was dissolved in distillated water and added to the calcined catalyst. Next, the mixture was heated at 80 °C with continuous stirring until all the water was evaporated. Finally, the prepared sample was dried at 120 °C for 12 h and further calcined at 350 °C for 3 h.

2.2 Catalyst Characterization

The specific surface areas and total pore size of catalysts were measured using a Nova 2200e Quantachrome gas adsorption–desorption apparatus with nitrogen gas adsorption at 77 K. The Brunauer–Emmett–Teller (BET) method was used to determine the specific surface areas and Barrett–Joyner–Halenda (BJH) and Non-Local Density Functional Theory (NL-DFT) methods were used to determine the pore size distribution of the catalysts. NL-DFT method that provides a microscopic treatment of sorption phenomena in micro and mesopores on a molecular level by statistical mechanics was used to pore analysis of the support materials used in this study beside BJH method.

Powder X-ray diffraction (XRD) analysis was performed using Rigaku X-ray Diffractometer (Model, Miniflex) with XuKα (30 kV, 15 mA, $\lambda = 1.54051$ Å).

XPS spectra were recorded using a SPECS spectrometer with a PHOIBOS-DLD hemispherical energy analyzer and a monochromatic Al Kα X-ray irradiation ($h\nu = 1{,}486.74$ eV, 400 W). Before XPS analysis, all samples were calcined at 753 K for 10 h under atmospheric conditions. The powder samples were placed on Cu-based conductive sticky tape. An e-beam flood gun was used for charge compensation during the XPS analysis. The flood gun parameters were chosen to be appropriate for compensating the binding energy (B.E.) shifts and peak width broadening. Thus, e-beam flood gun was operated using 5 eV electron energy and 70 μA emission current. All spectra were calibrated using the Si2p signal of the silica support material located at 103.3 eV.

FTIR measurements were carried out in transmission mode in a batch-type catalytic reactor coupled to an FTIR spectrometer (Bruker Tensor 27). FTIR spectra were recorded using a Hg–Cd–Te (MCT) detector. The samples were mounted into the IR cell equipped with optically-polished BaF_2 windows. About 20 mg of finely ground powder sample was pressed onto a high-transmittance, lithographically-etched fine tungsten grid which was mounted on a sample holder assembly, attached to a ceramic vacuum feed through. A K-type thermocouple was spot-welded to the surface of a thin tantalum plate attached on the W-grid to monitor the sample temperature. The sample temperature was controlled within 298–1,100 K via a computer-controlled DC resistive heating system using the voltage feedback from the thermocouple. After having mounted the sample in the IR cell, sample was gradually heated to 373 K in vacuum and kept at that temperature for 12 h before the experiments in order to ensure the removal of water from the surface.

2.3 Activity Tests

Catalyst performance tests were carried out using a computer controlled array channel microreactor system which is described elsewhere [40]. In this microreactor system, up to 80 catalyst samples could be screened in a parallel fashion. In the current set of experiments, 20 catalyst candidates were tested in each screening experiment and a performance data point was obtained for each catalyst in about 3 min. In the array microreactors, reactant gases flow over the flat surfaces of the powder catalyst samples which are individually isolated within reactor channels where the flow regime is similar to that of a monolithic reactor. All experiments were performed using a 5 mg catalyst sample under atmospheric pressure and at a gas hourly space velocity (GHSV) of 20,000 h^{-1}, representing a differential reactor condition. Catalytic screening experiments were performed at a C_3H_6/O_2 molar ratio of 0.5 and at 300 °C. Helium is used as a carrier gas. Products in the reactor effluent streams were sampled and analyzed using a heated capillary sampling probe and an on-line gas chromatograph [Varian CP-4900 Micro GC with thermal conductivity detector, Porapak Q (10 m) and Molecular sieve 13X (10 m) columns]. The selectivity of PO is defined as the moles of carbon in PO divided by the moles of carbon in all of the carbon containing products. The selectivity of the other C_3 products, such as acrolein (AC), acetone (AT) and acetaldehyde (AD) were also calculated in the same way.

3 Results and Discussion

3.1 Activity Tests

In our preliminary combinatorial catalytic tests, several catalysts containing mono-, binary and ternary oxides were

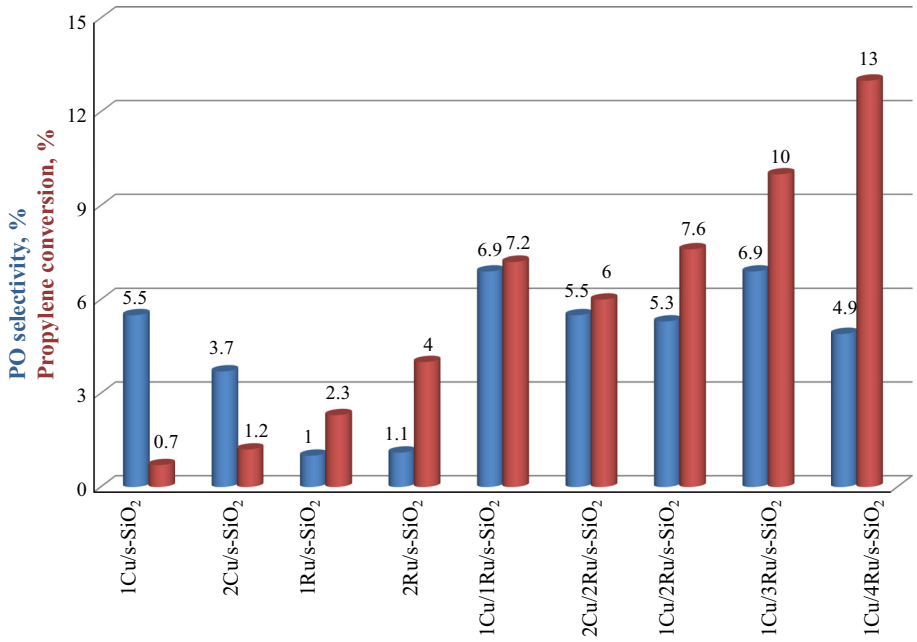

Fig. 1 Catalytic performance of mono and binary oxide Cu and Ru catalysts supported on s-SiO_2 (GHSV = 20,000 h^{-1}, Gas composition: C_3H_6:O_2 = 1:2, T = 300 °C)

screened to find a promising catalyst for direct oxidation of propylene to propylene oxide. To achieve this goal, first Ag and Cu salt precursors were loaded separately and together into the TiO_2, SiO_2, γ-Al_2O_3, and TiO_2–SiO_2 support materials prepared by using single step sol–gel method and into the α-Al_2O_3 by wet impregnation method [35]. Then monometallic Cu oxide catalysts promoted with various alkaline salt precursors were screened and observed relatively poor propylene conversion values which were typically below 3 % [39]. On the other hand, in some of the former reports in the literature such as the work of Seubsai and coworkers [37], 40–50 % PO selectivity at 10–20 % propylene conversion was reported over a new class of silica-supported multimetallic RuO_2–CuO_x–NaCl catalysts. Inspired by this work and the results obtained from our previous studies, single and binary combination of Cu, Ru, Mn and Ag oxide catalyst supported over silica material were prepared by wet impregnation method and screened into the high-throughput testing system. Among all the catalysts the most promising one was determined as the Cu–Ru oxide catalysts. Therefore in the current study, we focused on NaCl promoted catalysts containing Ru–Cu oxide which are prepared on different SiO_2 support materials.

The first part of the catalytic performance tests was devoted to the optimization of the relative Ru and Cu loadings on a given silica support material (i.e. s-SiO_2). In order to achieve this goal, different monometallic and binary oxide were prepared in the absence of NaCl, by varying the Cu and Ru loadings within 0–2 wt% and 0–4 wt%, respectively via sol–gel method. The amount of Cu and Ru precursor added into the support was calculated based on the Cu and Ru metal weight ratio. Therefore the symbolic designation of the catalysts was given according to the metal amount and not the oxide form (CuO and RuO_2) added into the support material as determined by XRD analysis. Propylene conversion and PO selectivity results of these catalytic tests are presented in Fig. 1. It is apparent in Fig. 1 that binary oxide catalysts typically reveal higher propylene conversion and PO selectivity with respect to that of their monometallic oxide counterparts indicating a synergistic interaction between Cu and Ru sites. Furthermore, Fig. 1 also points out that increasing the Ru loading in the binary oxide system while keeping the Cu metal content at a moderate level (e.g. 1 or 2 wt%) increases the catalytic yield performance with increasing propylene conversion. No significant change in PO selectivity is observed. From these results and previous report [37], through these experiments, 2 wt% Cu and 5 wt% Ru loadings were chosen as the optimum metal oxide loadings for the silica supported binary oxide catalysts for propylene oxidation.

As the second stage of the optimization approach, influence of the type of the silica support material on the catalytic performance was explored. Along these lines, we have prepared binary oxide catalysts on t-SiO_2, s-SiO_2 and c-SiO_2, which were loaded with 2 wt% Cu and 5 wt% Ru via wet impregnation (Fig. 2). The catalytic performance results presented in Fig. 2 suggests that the binary oxide catalyst supported on s-SiO_2 reveals the highest propylene conversion with a very poor PO selectivity (0.79 % PO yield), while the bimetallic catalyst supported on t-SiO_2

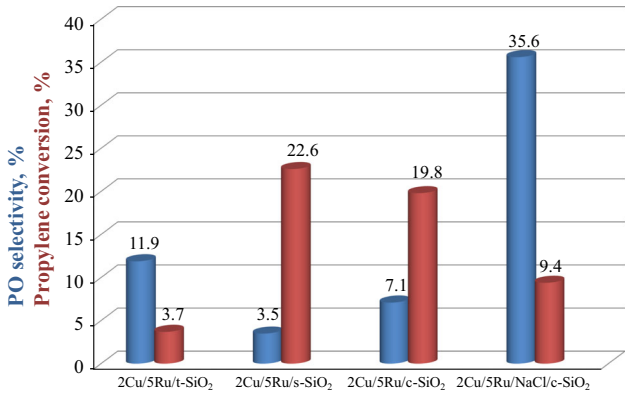

Fig. 2 Catalytic performance of 2 %Cu/5 %Ru catalyst supported on t-SiO_2, s-SiO_2 and c-SiO_2 and NaCl-promoted 2 %Cu/5 %Ru catalyst supported on c-SiO_2 (GHSV = 20,000 h^{-1}, Gas composition: C_3H_6:O_2 = 1:2, T = 300 °C)

Table 1 The specific surface area, pore size and pore volume of different silica support materials with and without Ru and Cu loading

Catalyst	Specific surface area (m^2/g)	Pore size (Å) (BJH)	Pore size (NLDFT)	Pore volume (cc/g)
c-SiO_2	96	34	51	0.15
2 %Cu/5 %Ru/c-SiO_2	82	34	70	0.23
t-SiO_2	936	34	35	0.57
2 %Cu/5 %Ru/t-SiO_2	799	30	22	0.49
s-SiO_2	718	37	52	0.31
2 %Cu/5 %Ru/s-SiO_2	605	34	38	0.27

presented the highest PO selectivity with a relatively poor propylene conversion (0.44 % PO yield). Preference of the s-SiO_2 supported material towards total combustion over selective oxidation may be attributed to the extensive micropores and thus high surface area of this material as given in Table 1. The residence time of the partial oxidation products in the micropores is increased facilitating the total oxidation process. On the other hand, the corresponding binary oxides catalyst supported on c-SiO_2 yielded a comparable propylene conversion to that of the s-SiO_2 catalyst without a drastic compromise in PO selectivity. Thus, in the light of these results, 2 %Cu/5 %Ru/c-SiO_2 was chosen in the second stage of the optimization approach as the preferred catalyst revealing both reasonable propylene conversion and PO selectivity gave the highest PO yield as 1.4 %.

As the final stage of the optimization approach, influence of a promoter on the 2 %Cu/5 %Ru/c-SiO_2 catalyst was investigated. For this purpose, we have used various alkali salt precursors such as NaCl, $NaNO_3$, KNO_3, KAc and LiCl as promoters. Figure 3 shows the catalytic performance of the promoted catalyst. As seen in Fig. 3,

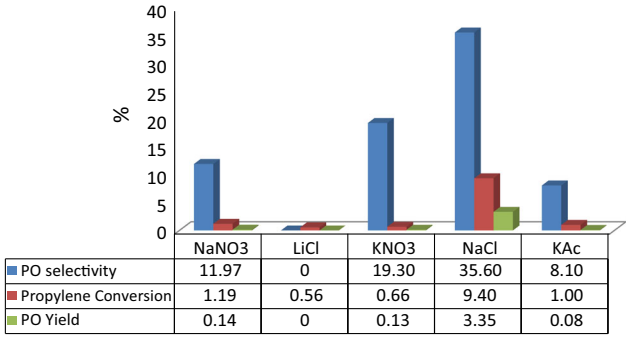

	NaNO3	LiCl	KNO3	NaCl	KAc
PO selectivity	11.97	0	19.30	35.60	8.10
Propylene Conversion	1.19	0.56	0.66	9.40	1.00
PO Yield	0.14	0	0.13	3.35	0.08

Fig. 3 Catalytic performance of 2 %Cu/5 %Ru catalyst modified by different alkaline metal salts (GHSV = 20,000 h^{-1}, Gas composition: C_3H_6:O_2 = 1:2, T = 300 °C)

NaCl enhanced the PO yield of Ru-Cu catalyst by increasing both overall conversion and selectivity more significantly than other promoters. The addition of KNO_3 also promoted PO selectivity but conversion remained at a very low level (0.7 %).The same situation has happened for KAc promoted catalyst with lower selectivity. The other sodium salt, $NaNO_3$, slightly increased PO selectivity as compared with Cu–Ru (7.1 % selectivity @ 19.8 % conversion) catalyst but a drastic decrease was observed in propylene conversion. Lithium chloride completely suppressed PO formation during reaction. Therefore, in the current text, we will particularly focus on the binary oxide catalysts promoted with the most effective promoter (i.e. NaCl). Corresponding catalytic conversion and selectivity results of the 2 %Cu/5 %Ru/1.75 %NaCl/c-SiO_2 catalyst in comparison with the 2 %Cu/5 %Ru/c-SiO_2 catalyst is shown again in Fig. 2. It can be seen in Fig. 2 that NaCl promotion has a significantly positive influence on the PO selectivity, while the increase in the PO selectivity is accompanied by some attenuation in the total propylene conversion.

Having determined the optimum ternary oxide catalyst (i.e. 2 %Cu/5 %Ru/1.75 %NaCl/c-SiO_2) using the combinatorial approach discussed above, a detailed product distribution analysis can be made for the relevant catalysts investigated in the current work. Figure 4 shows relative selectivity values of 2 wt% Cu and 5 wt% Ru monometallic oxide catalysts on c-SiO_2 as well as their NaCl promoted counterparts. For comparison, product distribution analysis of the 2 %Cu/5 %Ru/c-SiO_2 and 2 %Cu/5 %/Ru/1.75 % NaCl/c-SiO_2 catalysts are also given. The major products detected in the catalytic performance tests were CO_2, acetone (AT), acetaldehyde (AD), acrolein (AC) and propylene oxide (PO). As seen in Fig. 4, monometallic oxide 2 %Cu/c-SiO_2catalyst reveals a high selectivity towards AC while yielding a very low selectivity towards PO. This catalyst also leads to the highest selectivity towards AT among all of the other catalysts that were currently tested. On the other hand,

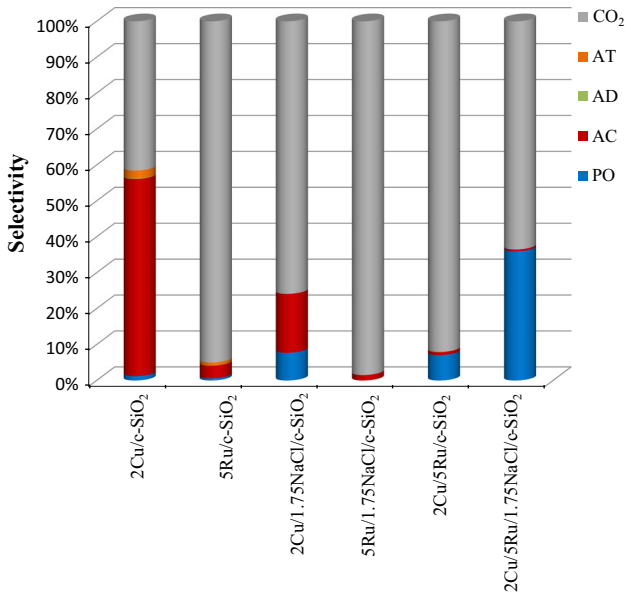

Fig. 4 Selectivity of the propylene oxidation reaction towards various products such as CO_2, acetone (AT), acetaldehyde (AD), acrolein (AC), propylene oxide (PO) over currently investigated catalysts (GHSV = 20,000 h^{-1}, gas composition: C_3H_6:O_2 = 1:2, T = 300 °C)

although the promotion of this catalyst with NaCl results in a noticeable increase in the PO selectivity at the expense of AC selectivity, overall PO selectivity is still considerably small.

Meanwhile, monometallic Ru oxide catalyst (i.e. 5 %Ru/c-SiO_2) presents a quite different behavior from its Cu counterpart. Figure 4 shows that 5 %Ru/c-SiO_2 catalyst leads to almost complete total oxidation of propylene to CO_2, with relatively minor amounts of AT, AC and PO production. Although NaCl promotion of the 2 %Cu/c-SiO_2 catalyst leads to an increase in the PO selectivity, an opposite trend is observed for the 5 %Ru/1.75 %NaCl/c-SiO2 catalyst, where the NaCl promotion drastically decreases the partial oxidation capability of the catalyst by significantly facilitating the total oxidation.

When the product distribution of the binary oxide 2 %Cu/5 %Ru/c-SiO_2 system is investigated, it is seen that the PO selectivity is comparable to that of the 2 %Cu/1.75 %NaCl/c-SiO_2 catalyst. On the other hand it is visible that the AC selectivity of the 2 %Cu/5 %Ru/c-SiO_2 system resembles to that of the 5 %Ru/1.75 %NaCl/c-SiO_2 catalyst, indicating an increasing tendency towards total oxidation to CO_2. Thus, it is apparent that NaCl promotion suppresses the AC production pathways to a great extent for both of the 2 %Cu/c-SiO_2 and 5 %Ru/c-SiO_2 monometallic systems. Finally, the NaCl promotion of the 2 %Cu/5 %Ru/c-SiO_2 system yields the highest PO selectivity among all of the currently investigated samples.

3.2 Characterization

The most effective catalyst in the direct oxidation of propylene to PO synthesis was determined by the selection of the optimum metal–metal ratio, silica support material and loading of the promoter by combinatorial screening method. 5 %Ru–2 %Cu-NaCl/c-SiO_2 catalyst showed the highest performance among the screened catalysts. The second stage of the study was followed by characterization of this catalyst with several methods to clarify the effect of each parameter on the physicochemical and electronic structure of the catalyst.

The commercial silica support material (c-SiO_2) with (2 %Cu–5 %Ru) and without metal loading revealed a type IIb adsorption isotherm while corresponding t-SiO_2 and s-SiO_2 samples showed type IV adsorption isotherms(Fig. 5).The adsorption/desorption hysteresis loop corresponding to commercial silica (c-SiO_2) is close to H4 type in terms of IUPAC classification [41]. A broad hysteresis loop is observed for the silica synthesized with sol–gel method (s-SiO_2), showing a desorption branch which is much steeper than the adsorption branch suggesting the filling and evacuation of the mesopores by capillary condensation. The relatively reversible adsorption isotherm of the t-SiO_2 sample indicates a type IVc isotherm which is associated with the reversible filling/evacuation of uniform cylindrical-like pores [41]. Addition of Ru and Cu metals into the support materials (Table 1) caused a decrease in the specific surface areas, pore sizes and volume adsorbed of the t-SiO_2 and s-SiO_2 materials most probably due to the partial plugging of the pores with metal particles while there is an increase in the pore volume of the c-SiO_2 at the constant pore size. NL-DFT analysis provides a much better interpretation about pore size analysis.

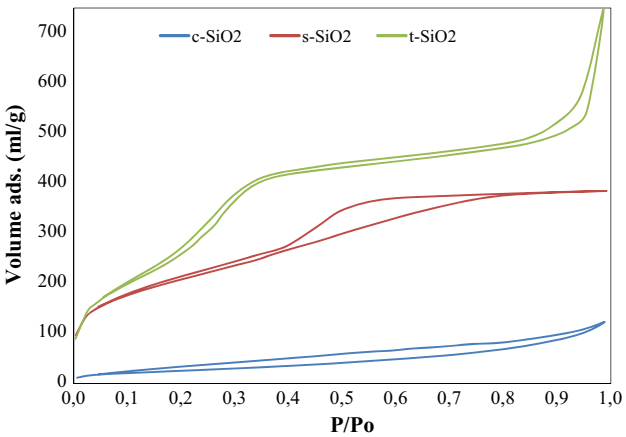

Fig. 5 N_2 adsorption/desorption isotherms of c-SiO_2, s-SiO_2 and t-SiO_2 support materials

In addition to the specific surface area analysis, the micropore analysis of the samples was made by Non-Local Density Functional Theory (NL-DFT) model.DFT analysis of samples showed that the ratio of cumulative surface area of s-SiO_2 material up to a pore width of 20 Å is 27 % while this value is zero for t-SiO_2 and c-SiO_2 materials. This result is in line with the poor PO selectivity over s-SiO_2 supported catalysts which can be explained by the limited diffusion of the oxygenated products out to the bulk gas phase, favoring total oxidation inside the micropores.

Structure of the Cu or Ru oxide containing monometallic catalysts, Ru-Cu binary oxidecatalysts as well as NaCl promoted Ru–Cu trimetallic catalysts were also investigated with XRD (Fig. 6). These samples revealed characteristic diffraction signals of RuO_2($2\theta = 28.49$, 35.59, 55.65, 67.30°), CuO ($2\theta = 35.70$, 38.95°) and NaCl ($2\theta = 31.81$, 45.54°) phases. Thus, XRD results suggested that Ru and Cu existed in oxidic forms on the freshly prepared catalysts, while Na was found to form crystalline NaCl. The particle sizes of CuO and RuO_2 remained almost constant (20 nm for RuO_2 and 28 nm for CuO) according to Scherrer equation after modification with NaCl. NaCl has no effect on the size and distribution of the oxide over support surface.

The structure of the 5 %Ru/c-SiO_2, 2 %Cu/c-SiO_2, 5 %Ru-2 %Cu/c-SiO_2, and 5 %Ru–2 %Cu-NaCl/c-SiO_2 catalysts were also analyzed by XPS (Figs. 7, 8). The Ru3d (i.e. the main XPS signal of Ru) signal in XPS overlaps with the intense C1s signal. Therefore, determination of the Ru oxidation states using the Ru3d region, particularly for low Ru loadings, is non-trivial. Thus, for the currently analyzed samples, Ru3p region was investigated (Fig. 7). Figure 7 shows that a poor and an asymmetric $Ru3p_{3/2}$ feature is observed at a BE of ~463 eV which is attributed to the RuO_2 species in agreement with the XRD data. The higher BE shoulder at 465–466 eV can be attributed to hydrated RuO_2 ($RuO_2{\cdot}xH_2O$) [42, 43].The extra feature in the spectrum of 5 %Ru–2 % Cu-NaCl/c-SiO_2 sample (a) at 498 eV is associated with the Auger signal of Na.

The Cu2p XP spectra of 5 %Ru–2 %Cu-NaCl/c-SiO_2, 2 %Cu/c-SiO_2, and 5 %Ru-2 %Cu/c-SiO_2 samples are presented in Fig. 8. Cu2p XP spectrum of the 5 %Ru-2 %Cu-NaCl/c-SiO_2 sample yields a $Cu2p_{3/2}$ peak at 933 eV, which is consistent with the presence of CuO species [44, 45]. On the other hand, Cu2p XP spectra of the (NaCl-free) 2 % Cu/c-SiO_2, and 5 %Ru–2 %Cu/c-SiO_2 samples reveal a strong differential charging behavior, yielding a significant $Cu2p_{3/2}$ BE shift of c.a. +5 eV. This detrimentally large differential charging behavior, which is extremely sensitive to the flood gun charge compensation parameters, is observed only in the absence of NaCl and is most likely due to the poor electrical conductivity at the Cu/SiO_2 or Cu/Ru/SiO_2 interfaces. As a result of this drastic differential charging, Cu 2p BE values of the NaCl-free samples are shifted out of the regular Cu 2p BE window. The changing of the flood gun electron beam energy leads to a moderate $Cu2p_{3/2}$ peak shift (up to 3 eV), while BE values of the Ru and Si signals are not altered by this change. These results clearly demonstrate the complex differential charging behavior of the NaCl-free samples and the strong dependence of the Cu2p XPS signal to the charge compensation parameters. Interestingly, the presence of the NaCl promoter drastically facilitates the charge compensation efficiency of the flood gun, shifting

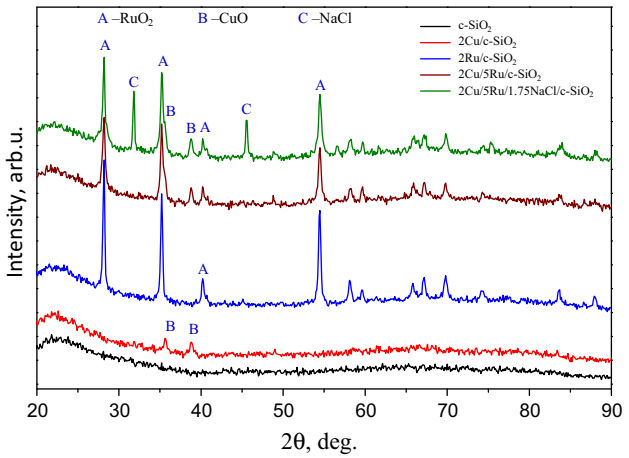

Fig. 6 XRD profiles of c-SiO_2, 2 %Cu/c-SiO_2, 2 %Ru/c-SiO_2, 2 %Cu/5 %Ru/c-SiO_2 and 2 %Cu/5 %Ru/1.75 %NaCl/c-SiO_2 samples

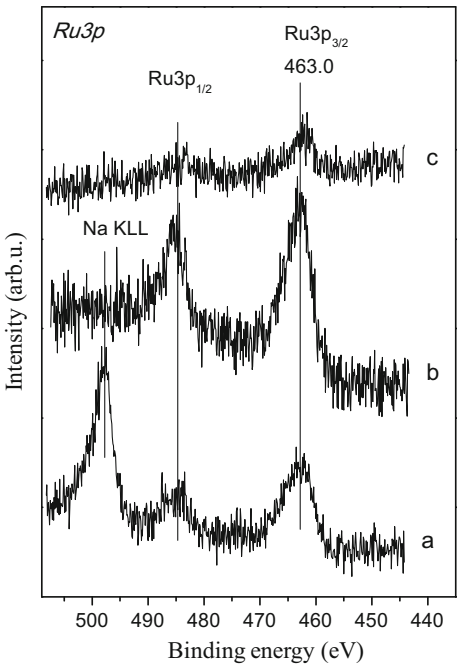

Fig. 7 Ru3p XP spectra of the calcined *a* 2 %Cu/5 %Ru/1.75 %NaCl/c-SiO_2, *b* 2 %Cu/5 %Ru/c-SiO_2 and *c* 5 %Ru/c-SiO_2 samples

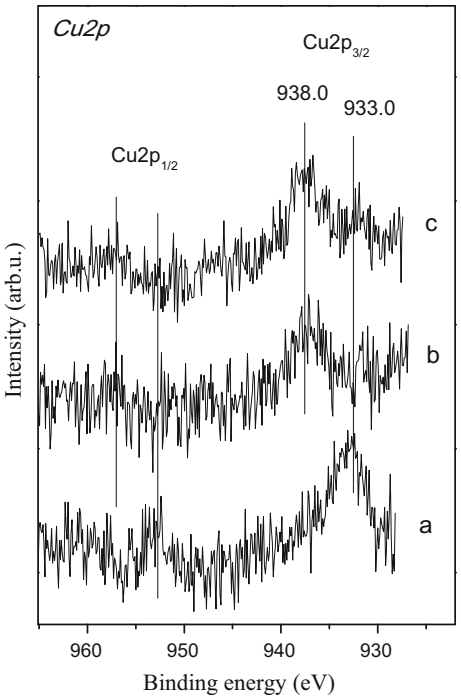

Fig. 8 Cu2p XP spectra of the calcined *a* 2 %Cu/5 %Ru/1.75 %NaCl/c-SiO_2, *b* 2 %Cu/c-SiO_2 and *c* 2 %Cu/5 %Ru/c-SiO_2 samples

the Cu2p BE back to the regular Cu2p energy window. Apparently, NaCl functions as a promoter enabling the charge transfer at the Cu/SiO_2 and/or Cu/Ru/SiO_2 interface preventing the charge build up on the surface during the XPS analysis.

In other words, although RuO_2 phase does not seem to reveal any indication of severe differential charging (i.e. charge build-up), Cu2p signal for NaCl-free samples disclose a severe and a remarkable amount of charge build-up on the CuO sites or at the CuO/SiO_2 interface. These two strikingly different differential charging behaviors of Ru and Cu sites on the same binary oxide catalyst surface suggest that in the absence of NaCl, Ru and Cu sites on the binary oxide catalyst are very well dispersed but probably not in a direct physical contact. Unlike the behavior described above, on the NaCl-promoted samples, CuO sites seem to be readily charge-compensated suggesting that NaCl functions as a structural promoter preventing the charge build-up at the Cu-SiO_2 and Cu-/Ru-SiO_2 interfaces.

Nature of the transition metal adsorption sites on the catalytic systems were also analyzed by FT-IR spectra obtained after CO(g) adsorption and saturation at 323 K over the catalyst surfaces. FT-IR analysis was performed for H_2-treated and un-treated 2 %Cu/c-SiO_2, 5 %Ru/c-SiO_2, 2 %Cu–5 %Ru/c-SiO_2, and 2 %Cu–5 %Ru/1.75 %NaCl/c-SiO_2 catalyst samples at 323 K.

The un-treated catalysts (where Ru and Cu sites exit in oxide form) showed negligible CO adsorption signal in FT-IR suggesting a relatively weak CO adsorption capability (data not shown here).

However, an interesting result was obtained for H_2-treated samples. Figure 9 presents the FT-IR spectra obtained after CO(g) adsorption on 2 %Cu/c-SiO_2, 5 %Ru/c-SiO_2, 2 %Cu–5 %Ru/c-SiO_2, and 2 %Cu–5 %Ru/1.75 %NaCl/c-SiO_2 samples at 323 K. Prior to CO adsorption, samples were treated with 10 Torr of H_2(g) at 473 K for 15 min. For the 2 %Cu/c-SiO_2 sample, the major vibrational feature is the signal at 2,124 cm^{-1}which is attributed to Cu^+–CO species. It was observed that for the H_2-treated samples (Fig. 9) CO probe molecule adsorbed strongly on the Cu^+ sites [38, 46].The Cu^{2+}–CO species which are also detectable are associated with the minor vibrational feature at 2,240 cm^{-1} [46, 47].

The CO adsorption on the 5 %Ru/c-SiO_2 sample (Fig. 8, spectra b–d) leads to the appearance of some characteristic vibrational bands such as the shoulder around 2,120–2,140 cm^{-1} (Fig. 8b) associated with CO chemisorbed over reduced Ru^0 sites [48]. The band at 2,067 cm^{-1} has been previously assigned to $Ru(CO)_3$ species on metallic Ru centers in the literature [49]. The broad feature at about 1,987 cm^{-1} has been assigned to CO adsorbed on coordinatively unsaturated Ru sites (i.e. Ru defect sites) and/or to

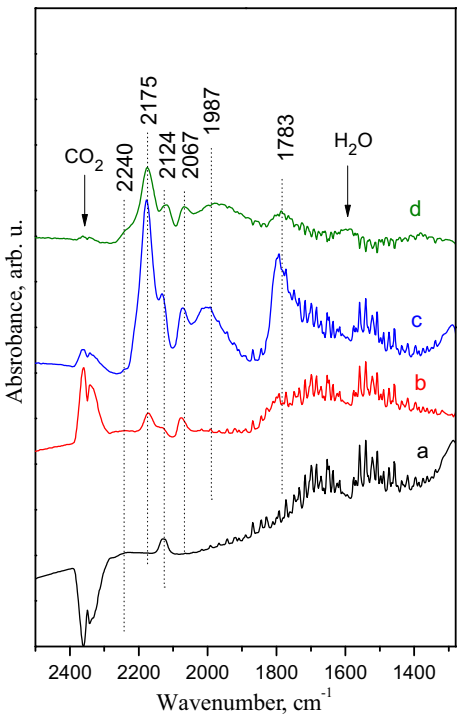

Fig. 9 In-situ FTIR spectra acquired after CO adsorption on *a* 2 %Cu/c-SiO_2, *b* 5 %Ru/c-SiO_2, *c* 2 %Cu/5 %Ru/c-SiO_2 and *d* 2 %Cu/5 %Ru/1.75 %NaCl/c-SiO_2 samples (see text for details)

isolated Ru^0–CO species [50–52]. The band at 2,175 cm^{-1} can be attributed to Ru^{n+}–CO where $n > 2$ [49]. The IR feature at 1,783 cm^{-1} can be assigned to bridging carbonyls (i.e. Ru_2^0–CO) [50].

A comparison of the spectra (a), (b) and (c) in Fig. 9 suggests that going from monometallic (i.e. 2 %Cu/c-SiO_2 and 5 %Ru/c-SiO_2) to a binary oxidecatalyst (2 %Cu–5 %Ru/c-SiO_2) increases not only the total CO adsorption on the overall catalyst surface but it also increases the CO uptake of the individual Ru and Cu sites. This observation points to the fact that Cu–Ru binary oxide catalyst reveals a synergistic behavior leading to the formation Cu^+ and Ru^{x+} sites even after H_2-treatment.

Finally, comparison of the spectra (c) and (d) also provides an important insight regarding the influence of the NaCl promoter on the 2 %Cu–5 %Ru/c-SiO_2, structure. It is apparent that the presence of NaCl decreases the intensities of all of the CO adsorption signals in the FT-IR data. This can be attributed to a strong interaction between NaCl and the active sites on the catalyst surface, in line with the current XPS results discussed above. CO adsorption experiments via FT-IR clearly demonstrate that binary oxide systems reveal a synergistic behavior by retarding the complete reduction of the metal oxide sites to metal sites and by forming a greater number of exposed adsorption sites. Furthermore, NaCl promoter directly interacts with the Cu and Ru active sites and modifies their adsorption properties towards CO.

The effect of the alkali promotion on the chemical states of copper in CuO_x/SiO_2 catalyst was investigated by He and co-workers under reaction condition through in situ XRD and CO-adsorbed FT-IR studies. They reported that Cu^+ species forms during reactions over modified and unmodified catalysts. They also reported that the presence of the alkali metal ions retards the reduction of the CuO as a result of the H_2-TPR analysis. The pulse-reaction experiments in this study showed that Cu^{2+}-containing catalysts yielded a low propylene conversion and a low PO selectivity while the presence of a low concentration of Cu^+ surface sites enhances the PO selectivity. On the other hand, it was also reported that for high Cu^+ to Cu^{2+} ratios, PO selectivity started to decrease while propylene conversion increased [38].

In the light of this study [38] and our current FT-IR results, it can be argued that on for 2 %Cu–5 %Ru/c-SiO_2 catalyst surface, Cu^+ and Ru^{+x} species are readily generated under reaction conditions (i.e. in the presence of C_3H_6 and O_2). As discussed previously, such a catalyst yielded a low PO selectivity with a high propylene conversion (7.1 % selectivity @ 19.8 % conversion). However when NaCl is added to the bimetallic oxides catalytic system, accessible number of Cu^+ and Ru^{+x} surface sites decreases as compared to the bimetallic oxides system decreasing the propylene conversion while increasing the PO selectivity (35.6 % selectivity @ 9.4 % conversion in Fig. 2).

As a conclusion, the reason behind the positive effect of NaCl addition in the Ru-Cu catalytic performance can be further elaborated in the light of the current XPS and in situ FT-IR experiments. XPS experiments (Figs. 7, 8) clearly demonstrate the drastic alterations in the structure of the 2 %Cu/5 %Ru/c-SiO_2 surface upon NaCl addition, as expected from an promoter. On the other hand, current in situ FTIR data (Fig. 9, spectrum *d*) for H_2-treated catalysts also point to the fact that NaCl promotion decreases the total number of CO-adsorption sites (i.e. Cu^+ and Ru^{+x} surface species). Thus, it is clear that although NaCl functions as a structural promoter facilitating the partial oxidation pathways over total oxidation (i.e. CO_2 production), NaCl also decreases the overall propylene conversion by decreasing the number of Cu^+ and Ru^{+x} sites generated during the reaction (Fig. 2).

4 Conclusions

In this study, a combinatorial approach was used in order to investigate an alkali salt-promoted binary oxide catalyst having an improved catalytic performance in the propylene partial oxidation. In order to find the optimum catalyst formulation, first the relative Cu (0–2 wt%) and Ru (0–5 wt%) loadings of the prepared catalysts were varied overs-SiO_2 support material, where it was found that 2 %Cu/5 %Ru/s-SiO_2 system revealed the best performance among the synthesized catalyst set in the micro reactor-based activity/selectivity tests. As the next step, influence of the nature of the silica support material on the catalytic performance was investigated by comparing the catalytic performances of 2 %Cu/5 %Ru/t-SiO_2, 2 %Cu/5 %Ru/s-SiO_2 and 2 %Cu/5 %Ru/c-SiO_2 catalysts. These experiments suggested that 2 %Cu/5 %Ru/c-SiO_2 catalyst yielded the most preferable performance with a high propylene conversion and a high PO selectivity. As the final step of this screening tests, several alkali salts (1.75 wt%) were incorporated into the 2 %Cu/5 %Ru/c-SiO_2 catalyst. It was observed that NaCl promotion significantly increased the PO selectivity which was accompanied by some attenuation in the total propylene conversion. These findings were explained in the light of the current XPS and in situ FTIR data. Along these lines, it was proposed that the 2 %Cu/5 %Ru/c-SiO_2 binary oxide system revealed a greater number of exposed active Cu^+ and Ru^{+x} surface sites with respect to that of the monometallic systems, combined (i.e. 2 %Cu/c-SiO_2 and 5 %Ru/c-SiO_2). Although NaCl addition is likely to decrease the total number of exposed Cu^+ and Ru^{+x} active surface sites, promotional effect of NaCl leads to an enhanced PO selectivity. Beside it was found

that an addition of 1.75 wt% NaCl has no effect on the particle size of the Cu and Ru oxides according to XRD analysis.

Acknowledgments This research was supported in part by TÜBİTAK through MAG Project No: 108T378. High throughput testing facilities at UCLA were provided by Prof. Selim Senkan. E.O. acknowledges support from Turkish Academy of Sciences (TUBA) through the "Outstanding Young Investigator" Grant. E.V. acknowledges RFBR (Russia) #12-03-91373-CT_a, for financial support.

References

1. Monnier JR (2001) Appl Catal 221:73
2. Nijhuis TA, Makkee M, Moulijn JA, Weckhuysen BM (2006) Ind Eng Chem Res 4:3447
3. Clerici MG, Bellussi G, Romano U (1991) J Catal 129:159
4. Zuwei X, Ning Z, Yu S, Kunlan L (2001) Science 292:1139
5. Kamata K, Yonehara K, Sumida Y, Yamaguchi K, Hikichi S, Mizuno N (2003) Science 300:964
6. Wang R, Guo X, Wang X, Hao J, Li G, Xiu J (2004) J Appl Catal A 261:7
7. Hayashi T, Tanaka K, Haruta M (1988) J Catal 178:566
8. Sinha AK, Seelan S, Tsubota S, Haruta M (2004) Angew Chem Int Ed 43:1546
9. Chowdhury B, Bravo-Sarez JJ, Date M, Tsubota S, Haruta M (2006) Angew Chem Int Ed 45:412
10. Ananieva E, Reitzmann A (2004) Chem Eng Sci 59:5509
11. Wang Y, Yang W, Yang LJ, Wang XX, Zhang QH (2006) Catal Today 117:156
12. Sacaliuc E, Beale AM, Weckhuysen BM, Nijhuis TA (2007) J Catal 248:235
13. Stangland EE, Stavens KB, Andres RP, Delgass WN (2000) J Catal 191:332
14. Qi C, Akita T, Okumura M, Haruta M (2001) Appl Catat A 218:81
15. Zwijnenburg A, Makkee M, Moulijn JA (2004) Appl Catal 270:49
16. Lu GZ, Zuo XB (1999) Catal Lett 58:67
17. Lu J, Luo M, Lei H, Li C (2002) Appl Catal A 237:11
18. Palermo A, Husain A, Tikhov M, Lamber RM (2002) J Catal 207:331
19. Zemicheael F, Palermo A, Tikhov M, Lambert RM (2002) Catal Lett 80:93
20. Jin G, Lu G, Guo Y, Guo Y, Wang J, Liu X (2003) Catal Lett 87:249
21. Takahashi A, Hamakawa N, Nakamura I, Fujitani T (2005) Appl Catal A 294:34
22. Lu J, Bravo-Suárez JJ, Takahashi A, Haruta M, Oyama ST (2005) J Catal 232:85
23. Lu J, Bravo-Suárez JJ, Haruta M, Oyama ST (2006) Appl Catal A 302:283
24. Yao W, Guo Y, Liu X, Guo Y, Wang Y, Wang Y, Zhang Z, Lu G (2007) Catal Lett 119:185
25. Lei Y, Mehmood F, Lee S, Greeley J, Lee B, Seifert S, Winans RE, Elam JW, Meyer RJ, Redfern PC, Teschner D, Schlögl R, Pellin MJ, Curtiss LA, Vajda S (2010) Science 328:224
26. Suo Z, Jin M, Lu J, Wei Z, Li C (2008) J Nat Gas Chem 17:184
27. Wang R, Guo X, Wang X, Hao J (2003) Catal Lett 90:57
28. Wang R, Hao J, Guo X, Wang X, Liu X (2004) Stud Surf Sci Catal 154:2632
29. Wang Y, Chu H, Zhu W, Zhang Q (2008) Catal Today 131:496
30. Lambert RM, Williams FJ, Cropley RL, Palermo A (2005) J Mol Catal A 228:27
31. Torres D, Lopez N, Illas F, Lambert RM (2007) Angew Chem Int Edit 46:2055–2058
32. Kizilkaya AC, Senkan S, Onal I (2010) J Mol Catal A 330:107
33. Vaughan OPH, Kyriakou G, Macleod N, Tikhov M, Lambert RM (2005) J Catal 236:401
34. Zhu W, Zhang Q, Wang Y (2008) J Phys Chem C112:7731
35. Onal I, Düzenli D, Seubsai A, Kahn M, Seker E, Senkan S (2010) Top Catal 53:92
36. Kahn M, Seubsai A, Onal I, Senkan S (2010) Comb Chem High Throughput Screen 13:67
37. Seubsai A, Kahn M, Senkan S (2011) Chem Cat Chem 3:174
38. He J, Zhai Q, Zhang Q, Deng W, Wang Y (2013) J Catal 299:53
39. Duzenli D, Seker E, Senkan S, Onal I (2012) Catal Lett 142:1234
40. Senkan S (2001) Angew Chem Int Ed 40:312
41. Rouquerol F, Rouquerol J, Sing K (1999) Adsorption by powders and porous solids principles, methodology and applications. Academic Press, San Diego
42. Chetty R, Xia W, Kundu S, Bron M, Reinecke T, Schuhmann W, Muhler M (2009) Langmuir 25:3853
43. Zeng Q, Zheng L, Zeng J, Liao S (2012) J Power Sources 205:201
44. Peebles DE, Peebles HC, Ohlhausen JA (1998) Colloids Surf A 144:89
45. Lee S, Song D, Kim D, Lee J, Kim S, Park IY, Choi YD (2004) Mater Lett 58:342
46. Hadjiivanov K, Knözinger H (2001) Phys Chem Chem Phys 3:1132
47. Busca G (1987) J Mol Catal 43:225
48. Yokomizo GH, Louis C, Bell AT (1989) J Catal 120:1
49. Sayan S, Kantcheva M, Suzer S, Uner DO (1999) J Mol Struct 480–481:241
50. Kantcheva M, Sayan S (1999) Catal Lett 60:27
51. Guglielminotti E, Bond GC (1990) J Chem Soc Faraday Trans 86:979
52. Robbins JL (1989) J Catal 115:120